Magnetic fields, non-thermal radiation and particle acceleration in colliding winds of WR-O stars

D. Falceta-Gonçalves[1]

[1]*Escola de Artes, Ciências e Humanidades, Universidade de São Paulo, Rua Arlindo Bettio 1000, CEP 03828-000, São Paulo, Brazil*

Non-thermal emission has been detected in WR-stars for many years at long wavelengths spectral range, in general attributed to synchrotron emission. Two key ingredients are needed to explain such emissions, namely magnetic fields and relativistic particles. Particles can be accelerated to relativistic speeds by Fermi processes at strong shocks. Therefore, strong synchrotron emission is usually attributed to WR binarity. The magnetic field may also be amplified at shocks, however the actual picture of the magnetic field geometry, intensity, and its role on the acceleration of particles at WR binary systems is still unclear. In this work we discuss the recent developments in MHD modelling of wind-wind collision regions by means of numerical simulations, and the coupled particle acceleration processes related.

1 Introduction

Wolf-Rayet (WR) stars represent a phase of the evolution of a massive star. Most of these objects are known to be in binary systems, making them a very interesting laboratory for the study of shocks in the space. This because the winds of massive stars are fast ($u_{\mathrm{wind}} \sim 1000 - 3000 \mathrm{km\ s}^{-1}$) and, in the case of luminous blue variables (LBVs) and WR stars, very massive as well ($\dot{M} \sim 10^{-7} - 10^{-4} \mathrm{M}_\odot \mathrm{\ yr}^{-1}$). When two (or more) massive stars form an orbiting system their winds are likely to shock violently, resulting in a vast sort of interesting phenomena, e.g. strong x-ray emission and high energy physics (see e.g. Eichler & Usov 1993; Pittard & Dougherty 2006; Abraham & Falceta-Gonçalves 2010; Reitberger et al. 2014).

Among the most intriguing processes involving shocks at massive binary systems is particle acceleration. Synchrotron emission at large wavelengths have been observed in several WR binaries, revealing both the existence of relativistic particles and strong magnetic fields. Since current models of particle acceleration depends on the magnetization of the shocks, the study of the evolution of the magnetic fields in wind-wind collision regions is crucial.

In this work we present the main results of recent magneto-hydrodynamical numerical simulations of wind-wind collisions. We also briefly discuss the implications of such modelling on the understanding of particle acceleration in such objects.

2 Modelling

In order to obtain the dynamical evolution of the shock region of the massive binary system we have employed a number of magneto-hydrodynamical (MHD) numerical simulations. The simulations were performed solving the set of ideal MHD equations, in conservative form, as performed in Falceta-Gonçalves & Abraham (2012). The set of equations is complete with an explicit equation for the radiative cooling. Two distinct setups were studied, namely the cases where radiative cooling were neglected and included, for comparison. These different setups correspond to the cases where the cooling time is longer, or shorter, respectively, to the dynamical timescales of the flows at the shock region.

The initial setup used was chosen to represent the system of η Carinae, with wind mass loss rates for the two stars as $\dot{M}_1 \sim 2 \times 10^{-4}$ M$_\odot$ yr^{-1} and $\dot{M}_2 \simeq 10^{-5}$ M$_\odot$ yr^{-1}, and wind terminal velocity $v_1 \sim 700$ km s^{-1} and $v_2 \simeq 3 \times 10^3$ km s^{-1}, respectively (Falceta-Gonçalves et al. 2005; Abraham et al. 2005a,b; Abraham & Falceta-Gonçalves 2007; Falceta-Gonçalves et al. 2008). The orbit is set with a major semi-axis $a = 15$AU and eccentricity $e = 0.9$. The magnetic field of both stars is initially set as a dipole with surface polar intensity $B_0 = 1$G, weak compared to the thermal and kinetic terms of the winds.

3 Results

The numerical integration of each model was performed for 2 complete orbital periods, which corresponds to approximately 11 years. Irrespectively to the model, the amplification of magnetic field at the shock has been shown to be larger than the values predicted by the Rankine-Hugoniot jump conditions (Rocha da Silva et al. 2015). This occurs because the R-H jump conditions are computed for 1D solution of conservation equations, while the shock is multidimensional. It was already shown in Falceta-Gonçalves & Abraham (2012) that the flow of the post-shocked gas occurs mostly parallel to the field lines, reducing the local pressure and allowing further compression of the magnetic fields at the shock layers. Also, in the cases of strong cooling, this compression occurs even further, resulting in magnetic fields orders of magnitude larger that the predicted by R-H jump conditions.
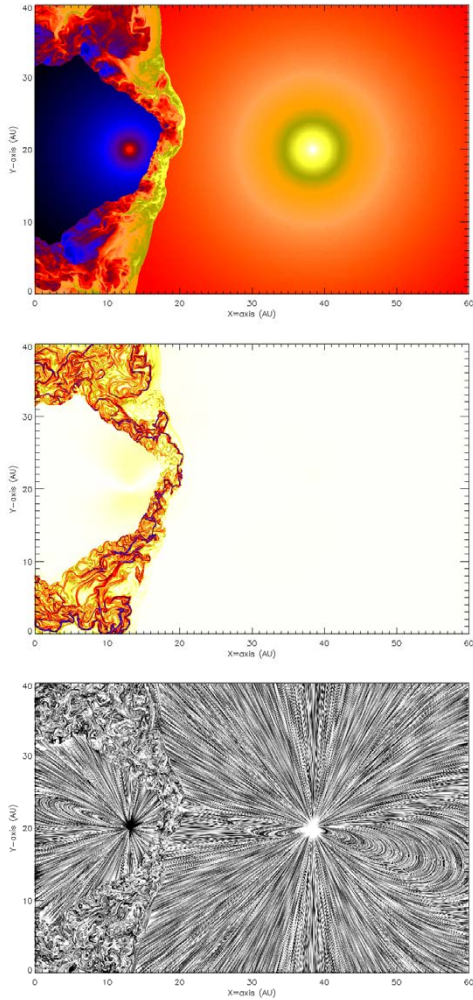
In Figure 1 we present the central slice of the model with radiative cooling at orbital phase 0.5, i.e. near apastron. The maps are shown for density (top), magnetic energy density (central) and line integral convolution (LIC) for the magnetic field orientation (bottom). The top panel shows that the standard picture of a two shock layers separated by a contact discontinuity is broken. Here the entrainment of material among the two layers is very efficient, as a consequence of the Nonlinear Thin Layer Instability. Several observations of the wind-wind collision region of massive binaries indicate them to be turbulent (Falceta-Gonçalves et al. 2006). This mixing property of turbulent flows is also responsible for the complex geometry of the magnetic field lines at the shock. Instead of accumulating at the contact discontinuity (Rocha da Silva et al. 2015),

high magnetic energy density regions are mixed, as shown in the central panel of this figure.
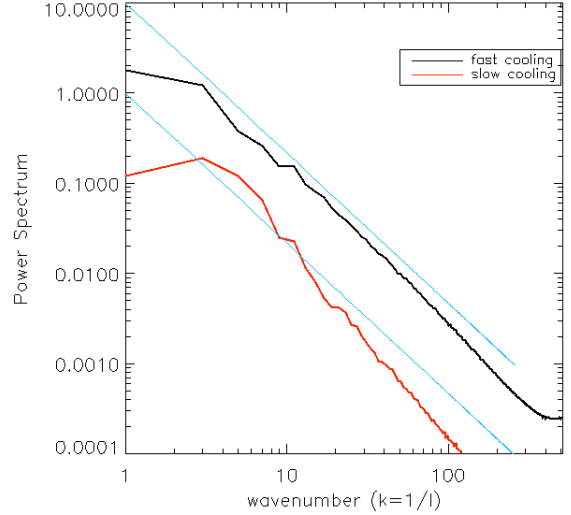

Fig. 2: Power spectrum of magnetic field for two different models, with and without radiative cooling included. Effects of cooling include the growth of local instabilities (e.g. nonlinear thin-layer instability) and turbulent dynamics.

The magnetic field orientation at the shock is absolutely chaotic, as seen in the bottom panel of Figure 1. Here we show the line integral convolution LIC technique applied for the magnetic field lines. The texture shown represents the orientation of the field lines, which are kept approximately dipolar for the surroundings of the stars. At the shock, one would expect a field parallel to the shock structure. Indeed, this is standard result for the adiabatic model. In the cooled case, turbulence at the shock region results in very complex geometry of B-field lines. The scaling of such complex distribution of magnetic field can be obtained from its power spectrum.

The turbulent power spectra of the magnetic field at the shock region obtained for the adiabatic and cooled models are shown in Figure 2. The plot shows the power spectra obtained for the adiabatic and cooled models, and the reference line for Kolmogorov scaling ($P_k \propto k^{-5/3}$). It is clear that the cooled model presents much larger power of turbulent components that the adiabatic model. Also, the slope obtained for the cooled model resembles well the typical energy cascade of Kolmogorov's turbulence, while the adiabatic model shows a steeper spectrum, as a consequence of a dominance of the more uniform (sheath-like) component (Falceta-Gonçalves et al. 2014).

3.1 B-n correlation at wind-wind shock regions

The correlation between the magnetic field energy density and the local gas density is typically used once equipartition between the magnetic and particle kinetics is assumed. This has been largely used by theorists so far in order to model the levels of magnetization of shock regions, as well as to predict the high energy content of particle distributions. However, as shown in Figure 3, the correlation between B and the gas density n is far from trivial.

Three clustering are visible, representing the stellar winds and the shocked region. The more diffuse and highly magnetized cluster of density corresponds to the shock. It is clear that any attempt to fit a $B \propto n^{\alpha}$ correlation is unsuccessful (Burkhart et al. 2009). Therefore, in order to properly model, for instance, the synchrotron emission from massive binaries, one needs to fully evolve the magnetic field as well as the acceleration of particles self-consistently.
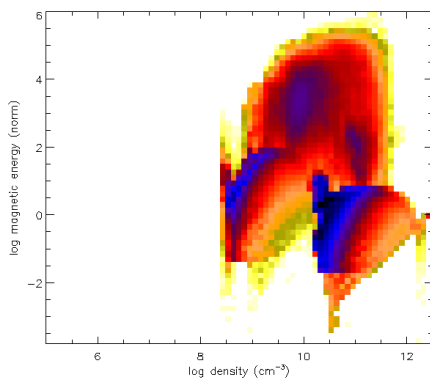

Fig. 3: 2D histogram of the model for the correlation between local density and the magnetic energy density. In general, assumption of equipartition $B^2 \propto \rho$ is used for the description of the non=thermal component of the shock region (see text), however we show that the situation is far more complex.

3.2 Particle acceleration

As pointed by Eichler & Usov (1993), the shock region of massive binaries may be ideal for particle acceleration to relativistic speeds. First order Fermi acceleration is commonly employed in such systems, which is efficient once the shock structure is uniform. If after each shock crossing the energy of the particle increases by a factor $\delta E/E \sim 2U/3c$, where U represents the upstream flow velocity, we obtain – for

the parameters of our simulations – an acceleration timescale (from keV to TeV) of $\tau_{\mathrm{acc}} \sim 10^4 - 10^5$s. Unfortunately, this is slow compared to particle diffusion time ($\tau_{\mathrm{diff}} \sim L/v_{\mathrm{part}}$), or even for collisions. Therefore, for the model of the system of eta Carinae, the 1st order Fermi process is not dominant.

However, we have shown that the shocked region is very turbulent. In such an environment particles should be accelerated to relativistic either by the 2nd order Fermi process or by electric fields arising from turbulent reconnection zones. In the 2nd order process the acceleration occurs as random collisions within the shock region, i.e. diffusion at timescales $\tau_{\mathrm{acc}} \sim Lc/ < \delta v^2 >$. For the turbulence parameters obtained from the simulations, $< \delta v^2 >^{1/2} \sim 100$km s^{-1} at $L \sim 10^9$cm, we obtained fast initial acceleration and saturation of relativistic particles with $N(E)dE \propto (E^{-2} - E^{-1})dE$, at maximum energy of $1 - 10$TeV.

References

Abraham, Z. & Falceta-Gonçalves, D. 2007, MN-RAS, 378, 309

Abraham, Z. & Falceta-Gonçalves, D. 2010, MN-RAS, 401, 687

Abraham, Z., Falceta-Gonçalves, D., Dominici, T., Caproni, A., & Jatenco-Pereira, V. 2005a, MN-RAS, 364, 922

Abraham, Z., Falceta-Gonçalves, D., Dominici, T. P., et al. 2005b, A&A, 437, 977

Burkhart, B., Falceta-Gonçalves, D., Kowal, G., & Lazarian, A. 2009, ApJ, 693, 250

Eichler, D. & Usov, V. 1993, ApJ, 402, 271

Falceta-Gonçalves, D. & Abraham, Z. 2012, MN-RAS, 423, 1562

Falceta-Gonçalves, D., Abraham, Z., & Jatenco-Pereira, V. 2006, MNRAS, 371, 1295

Falceta-Gonçalves, D., Abraham, Z., & Jatenco-Pereira, V. 2008, MNRAS, 383, 258

Falceta-Gonçalves, D., Jatenco-Pereira, V., & Abraham, Z. 2005, MNRAS, 357, 895

Falceta-Gonçalves, D., Kowal, G., Falgarone, E., & Chian, A. C.-L. 2014, Nonlinear Processes in Geophysics, 21, 587

Pittard, J. M. & Dougherty, S. M. 2006, MNRAS, 372, 801

Reitberger, K., Kissmann, R., Reimer, A., & Reimer, O. 2014, ApJ, 789, 87

Rocha da Silva, G., Falceta-Gonçalves, D., Kowal, G., & de Gouveia Dal Pino, E. M. 2015, MNRAS, 446, 104

D. Falceta-Gonçalves